# Correlation of ultrasonic scatterer size estimates for the statistical analysis and optimization of angular compounding

Anthony Gerig,[a] Quan Chen, James Zagzebski, and Tomy Varghese
*Department of Medical Physics, University of Wisconsin—Madison, 1300 University Ave. Rm. 1530, Madison, Wisconsin 53706*

(Received 15 October 2003; revised 8 March 2004; accepted 9 April 2004)

Ultrasonic scatterer size estimates generally have large variances due to the inherent noise of spectral estimates used to calculate size. Compounding partially correlated size estimates associated with the same tissue, but produced with data acquired from different angles of incidence, is an effective way to reduce the variance without making dramatic sacrifices in spatial resolution. This work derives theoretical approximations for the correlation between these size estimates, and the coherence between their associated spectral estimates, as functions of ultrasonic system parameters. A Gaussian spatial autocorrelation function is assumed to adequately model scatterer shape. Both approximations compare favorably with simulation results, which consider validation near the focus. Utilization of the correlation/coherence expressions for statistical analysis and optimization is discussed. Approximations, such as the invariance of phase and amplitude terms with angle, are made to obtain closed-form solutions to the derived spectral coherence near the focus and permit analytical optimization analysis. Results indicate that recommended parameter adjustments for performance improvement generally depend upon whether, for the system under consideration, the primary source of change in total coherence with rotation is phase term variation due to the change in the relative position of scattering sites, or field amplitude term variation due to beam movement.
 [DOI: 10.1121/1.1756615]

PACS numbers: 43.80.Vj, 43.80.Qf [FD] Pages: 1832–1841

## I. INTRODUCTION

Ultrasonic scatterer size estimation and imaging has proven to be both feasible and useful for the monitoring, diagnosis, and study of disease.[1–9] However, it is hampered by low signal-to-noise ratios, which ultimately result from the random placement of scatterers in tissue.[10–12] This difficulty is intrinsic to the majority of techniques used in ultrasonic imaging, including standard B-mode processing in the form of speckle.[13–15] One method that can be used to reduce the severity of this problem is to spatially compound partially correlated results which are associated with the same tissue, but which are produced with data that are taken from different angles of incidence. The application of spatial compounding to B-mode imaging has been investigated extensively, and has yielded excellent results.[16–19] As a result, many modern clinical scanners include a compounding option to reduce speckle and provide the additional benefit of improved specular reflector imaging. Recent work done by our group has been devoted to adapting the spatial compounding technique for use in elastography and parametric imaging that involves spectral analysis, such as scatterer size and attenuation imaging.[20] For the case of parametric imaging, either the power spectral estimates necessary for parameter estimation can be compounded beforehand, or parametric estimates can be generated for each angle of incidence and then averaged.

Much theoretical work, with implications for the statistical analysis and optimization of B-mode spatial compounding, has also been done.[16,18] Wagner *et al.* and O'Donnell *et al.* investigated the dependence of the rf signal and amplitude correlation upon experimental parameters. O'Donnell *et al.* used the results to explore optimizing transducer translation for compounding. However, because work concerned with the application of angular compounding to parametric imaging has been recent, the analogous theoretical research for signal power spectra and parameter estimates has not been done.

The purpose of the following is to develop a theoretical framework that, although pertinent for any type of tissue characterization involving power spectra, will permit statistical analysis and optimization in the application of angular compounding to scatterer size estimation and imaging in particular. Approximate expressions for both spectral coherence and size estimate correlation in terms of experimental parameters, including the angular separation between different incidence directions, are derived. Results of a comparison between these expressions and simulations are presented. A general discussion of the statistical analysis and optimization of angular compounding techniques applied to size estimation, given knowledge of the correlation as derived, ensues. Finally, further assumptions are made which yield analytic solutions to the expression for the spectral coherence, and, based upon the results, parameter adjustment recommendations for performance improvement are given.

## II. THEORY

### A. Spectral coherence

The essential quantity for determining the correlation between size estimates is the coherence between the Fourier

[a]Corresponding author. Electronic mail: algerig@wisc.edu

transforms of the rf (radio frequency) data segments used to generate those estimates. In general form, the Fourier transform of an rf data segment gated with a rectangular window is given approximately by[21]

$$V(\omega)\approx G(\omega)B(\omega)\omega^2\int_{\Delta\Omega} dr\,\gamma(\mathbf{r})A_t(\mathbf{r},\omega)A_{\mathbf{r}}(\mathbf{r},\omega), \quad (1)$$

where $\omega$ is the angular frequency, $G(\omega)$ is the complex transfer function for the transducer, $B(\omega)$ is the complex superposition coefficient corresponding to the insonifying pulse, and $A_t$ and $A_r$ are the field integrals (see the appendix), which include attenuation terms, corresponding to spatial point $\mathbf{r}$ (the origin at the transducer face) for transmit and receive, respectively. It is assumed that a linear, shift-invariant system is scanning a stationary, medium in which only incoherent scatter is significant. $\gamma(\mathbf{r})=[\kappa(\mathbf{r})-\kappa_0]/\kappa_0 -[\rho(\mathbf{r})-\rho_0]/\rho(\mathbf{r})$ is the reflectivity of the scattering medium, where $\kappa$ and $\rho$ are compressibility and density, and $\kappa_0$ and $\rho_0$ are their corresponding mean values for the medium.[22] $\Delta\Omega$ is the region of the medium which contributes significantly to the gated rf signal. It includes positions in space for which $2|\mathbf{r}|/c$ falls within the time gate, where $c$ is the speed of sound for the medium. Approximating the time gate as a spatial gate in this manner is viable given that the time duration of the system response for a single scatterer is short in comparison to the gate length. As a result, it is most accurate when broadband pulses are used.

Within this framework, reflectivity is a random variable with zero mean. The covariance between two Fourier transformed signal segments, obtained from the same medium but different transducer positions, is therefore given by

$$\begin{aligned}\langle V_1(\omega)V_2^*(\omega)\rangle\approx|G(\omega)B(\omega)|^2\omega^4\int\int_{\Delta\Omega_{1,2}} d\mathbf{r}_1 d\mathbf{r}_2 \\ \times A_t(T(\mathbf{r}_1),\omega)A_r(T(\mathbf{r}_1),\omega) \\ \times A_t^*(\mathbf{r}_2,\omega)A_r^*(\mathbf{r}_2,\omega) \\ \times\langle\gamma(\mathbf{r}_1)\gamma^*(\mathbf{r}_2)\rangle, \quad (2)\end{aligned}$$

where the spatial integration is done in the coordinate system defined by transducer position 2, and $T$ transforms coordinates in this system to those of the system defined by transducer position 1. In this instance, it is used to place the acoustic field generated at position 1 into the coordinate system defined by position 2. This formulation assumes that the acoustic field produced by the transducer is identical for positions 1 and 2. However, it can be easily adapted by changing the field integral for one of the positions to include cases where they are different. Making the change of integration variable, $\mathbf{r}_2=\mathbf{r}_1+\boldsymbol{\Delta}\mathbf{r}$, and invoking the approximation[21] often used in the far-field, $k|\mathbf{r}_1+\boldsymbol{\Delta}\mathbf{r}-\mathbf{r}'|\approx k|\mathbf{r}_1-\mathbf{r}'|+k\cdot\boldsymbol{\Delta}\mathbf{r}$ and $|\mathbf{r_1}+\boldsymbol{\Delta}\mathbf{r}-\mathbf{r}'|\approx|\mathbf{r_1}-\mathbf{r}'|$, yields

$$\begin{aligned}\langle V_1(\omega)V_2^*(\omega)\rangle\approx|G(\omega)B(\omega)|^2\omega^4 \\ \times\int_{\Delta\Omega_1} d\mathbf{r}_1 A_t(T(\mathbf{r}_1),\omega) \\ \times A_r(T(\mathbf{r}_1),\omega)A_t^*(\mathbf{r}_1,\omega)A_r^*(\mathbf{r}_1,\omega) \\ \times\int_{\Delta\Omega_2} R_\gamma(\boldsymbol{\Delta}\mathbf{r})e^{-2i\mathbf{k}\cdot\boldsymbol{\Delta}\mathbf{r}}d\boldsymbol{\Delta}\mathbf{r}, \quad (3)\end{aligned}$$

where $R_\gamma(\boldsymbol{\Delta}\mathbf{r})$ is the autocorrelation function of the reflectivity, is a function of $\Delta\mathbf{r}$ alone for statistically stationary media, and falls to zero quickly for media containing small scatterers.[22] It is, in general, the sharp decrease in this value with distance that makes the approximation described above appropriate. $\mathbf{k}$ (the magnitude denoted by $k$) is the wavenumber corresponding to the angular frequency, $\omega$, and has direction $(\mathbf{r}_1-\mathbf{r}')/|\mathbf{r}_1-\mathbf{r}'|$ where $\mathbf{r}'$ is the variable of integration in the field integrals. Assuming that the autocorrelation function possesses spherical symmetry, Eq. (3) can be simplified to

$$\begin{aligned}\langle V_1(\omega)V_2^*(\omega)\rangle\approx|G(\omega)B(\omega)|^2C(\omega)\omega^4 \\ \times\int_{\Delta\Omega_{1,2}} d\mathbf{r}_1 A_t(T(\mathbf{r}_1),\omega) \\ \times A_r(T(\mathbf{r}_1),\omega)A_t^*(\mathbf{r}_1,\omega)A_r^*(\mathbf{r}_1,\omega), \quad (4)\end{aligned}$$

where $C(\omega)$ is the Fourier transform of the autocorrelation function, and is directly related to the form factor for the medium.[22] As before, the integration is restricted to values of $\mathbf{r}_1$ for which signals from both fields fall into the time gate. The coherence between Fourier transformed segments is therefore given by

$$\rho_{1,2}(\omega)=\frac{\langle V_1(\omega)V_2^*(\omega)\rangle}{\sqrt{\langle|V_1(\omega)|^2\rangle}\sqrt{\langle|V_2(\omega)|^2\rangle}}\approx\frac{\int_{\Delta\Omega_{1,2}}d\mathbf{r}_1 A_t(T(\mathbf{r}_1),\omega)A_r(T(\mathbf{r}_1),\omega)A_t^*(\mathbf{r}_1,\omega)A_r^*(\mathbf{r}_1,\omega)}{\int_{\Delta\Omega}d\mathbf{r}|A_t(\mathbf{r},\omega)|^2|A_r(\mathbf{r},\omega)|^2}, \quad (5)$$

where it has been assumed that the time gates for the two positions are identical in duration and type. Assuming that the medium contains many independent scatterers per gated segment, the real and imaginary parts of the segment transforms are approximately jointly Gaussian distributed. As a result, the mathematical formalism pertaining to Gaussian distributed variables used by Wagner in determining speckle correlation also applies here, and the coherence between the periodogram power spectral estimates for the segments, given by $|V(\omega)|^2$, can be expressed by the simple formula[18]

$$\rho_S(\omega)=|\rho_{1,2}(\omega)|^2. \quad (6)$$

Although Eqs. (5) and (6) are valid for any two data segments taken from the same medium, the primary concern

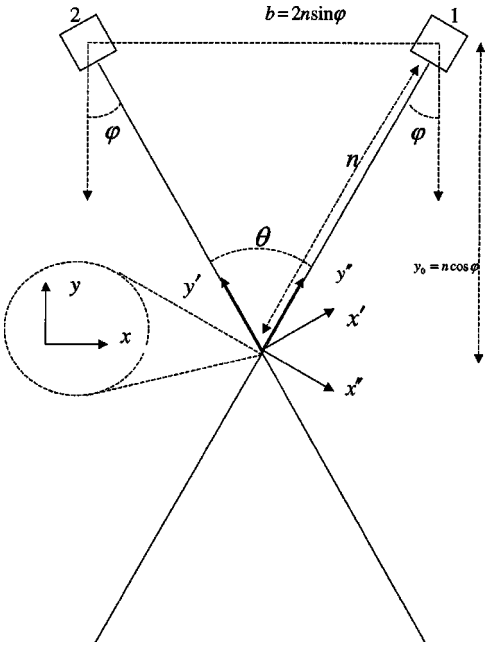


FIG. 1. The coordinate system used in deriving the spectral coherence between angled beamlines.

here is with the coherence between segments obtained from the same location but from different angles of incidence. For this case, if the spatial coordinate system for integration is redefined such that the origin is located at the transducer's axis of rotation, as illustrated in Fig. 1, then the transformation of Eq. (5) becomes a simple rotation about that axis where

$$x''=x'\cos\theta-y'\sin\theta,\quad y''=x'\sin\theta+y'\cos\theta, \tag{7}$$

and $\theta$ is the angular separation between positions 1 and 2. In general, Eq. (5) is not easy to calculate analytically due to the inherent difficulty of obtaining closed-form expressions for the acoustic fields involved, and to the complexity of those expressions as integrands when they are available in closed-form. However, it is possible to simplify the integral in certain cases. One of the simulations included in this paper is devoted to verifying Eq. (5) for one such case, namely, when the far-field approximation can be used. The field at the transmit focus of a transducer can be accurately represented by this approximation[23] and will receive particular attention here, although the approximation is appropriate in other instances as well. To further simplify matters for the simulation, attenuation will be neglected. Applying the far-field approximation to Eq. (5) yields

$$\rho_{1,2}(\omega)\approx\frac{\int_{\Delta\Omega_{1,2}}P(T(\mathbf{r}_1),\omega)P(\mathbf{r}_1,\omega)\frac{e^{2ik|T(\mathbf{r}_1)|}}{|T(\mathbf{r}_1)|^2}\frac{e^{-2ik|\mathbf{r}_1|}}{|\mathbf{r}_1|^2}d\mathbf{r}_1}{\int_{\Delta\Omega}P^2(\mathbf{r},\omega)\frac{1}{|\mathbf{r}|^4}d\mathbf{r}}, \tag{8}$$

where $P$ is the point-spread function (amplitude only) of the transducer, which can include terms for dynamic receive aperture and apodization. Assuming approximate field symmetry in the elevational direction such that integration in that direction is unnecessary, and applying the geometry of Fig. 1, where the rotation axis is perpendicular to the diagram and passes through the transducer transmit focus, gives

$$\rho_{1,2}(\omega)\approx\frac{\int_{\Delta\Omega_{1,2}}dx\,dy\,p(x\cos\varphi-y\sin\varphi,x\sin\varphi+y\cos\varphi,\omega)p(x\cos\varphi+y\sin\varphi,-x\sin\varphi+y\cos\varphi,\omega)}{\int_{\Delta\Omega}dx\,dy\,p^2(x,y,\omega)}$$
$$\times\frac{e^{2ik(\sqrt{(x-b/2)^2+(y_0-y)^2}-\sqrt{(x+b/2)^2+(y_0-y)^2})}\dfrac{1}{[(x-b/2)^2+(y_0-y)^2][(x+b/2)^2+(y_0-y)^2]}}{\dfrac{1}{[x^2+(n-y)^2]^2}}, \tag{9}$$

where $p(x,y,\omega)$ is the point-spread function when the coordinate system has been translated from the transducer face to the transmit focus, and half-angle transformations ($\varphi=\theta/2$) have been applied to both transducer positions rather than a full-angle transformation to position 1 alone. $b$ is the distance from position 1 to position 2 and $n$ is the distance from the transducer face to the transmit focus.

### B. Size estimate correlation

Size estimation generally involves dividing a spectral estimate obtained from a medium by a type of transfer function for the system used to gather the data, and an attenuation correction term.[1,4] What results is a backscatter estimate for the medium, which can be fit to theoretical curves, whose frequency dependencies are functions of scatterer size, to produce a size estimate. Several different theoretical models have been used to generate size estimates,[4] however, the emphasis here will be upon the Gaussian model for scatterer spatial autocorrelation functions (SAF). For this model, the size estimate (effective radius) corresponding to an individual backscatter estimate is given by[11]

$$\hat{a}^2 = \frac{-d_1^2 c^2 \Sigma_{\omega_{\min}}^{\omega_{\max}} (y(\omega)\omega^2 - \overline{y\omega^2})}{80 \Sigma_{\omega_{\min}}^{\omega_{\max}} (\omega^2 - \overline{\omega^2})^2}, \tag{10}$$

where $y(\omega) = 10 \ln(\hat{BSC}(\omega)/\omega^4)$, $d_1 \approx 3.1$ is a constant that relates the scatterer size to the characteristic length of the Gaussian SAF, and the summation is over discrete frequency values within the bandwidth of the transducer. Although backscatter estimates $(\hat{BSC}(\omega))$ at neighboring frequency points can, in general, be correlated (e.g., if zero-padding or nonrectangular gates are used in a spectral estimation), the assumption here will be that only uncorrelated terms have been included in the summation and that correlated terms have been discarded.

Assuming that a periodogram is used to generate spectral estimates for size estimation, the results from the preceding section can be used to determine the correlation between both backscatter and size estimates produced using correlated rf data segments. If knowledge of the associated system transfer function and attenuation is near perfect, then $\hat{S}(\omega) = f(\omega)\hat{BSC}(\omega)$, where $\hat{S}(\omega)$ is a power spectral estimate and $f(\omega)$ is dependent solely upon the transfer function and attenuation [includes all terms from Eq. (4) for a zero degree angle but $\omega^4 C(\omega)$]. The correlation between backscatter estimates is therefore given by

$$\begin{aligned}
&\rho_{\mathrm{BSC}}(\omega) \\
&= \frac{\frac{1}{f_1(\omega) f_2(\omega)} \langle (\hat{S}_1(\omega) - \langle \hat{S}_1(\omega) \rangle)(\hat{S}_2(\omega) - \langle \hat{S}_2(\omega) \rangle) \rangle}{\frac{1}{f_1(\omega)} \mathrm{std}(\hat{S}_1(\omega)) \frac{1}{f_2(\omega)} \mathrm{std}(\hat{S}_2(\omega))} \\
&= \rho_S(\omega),
\end{aligned} \tag{11}$$

where the subscripts, as previously, refer to different locations in the same medium. From here, the approximation[24]

$$\begin{aligned}
\mathrm{cov}(\hat{a}_1, \hat{a}_2) \approx \sum_{\omega_i} \sum_{\omega_j} &\left( \frac{\partial \hat{a}_1}{\partial \hat{BSC}_1(\omega_i)} \right) \left( \frac{\partial \hat{a}_2}{\partial \hat{BSC}_2(\omega_j)} \right) \\
&\times \mathrm{cov}(\hat{BSC}_1(\omega_i), \hat{BSC}_2(\omega_j))
\end{aligned} \tag{12}$$

can be used to determine the correlation between size estimates, where each partial derivative is evaluated at the expected value of the associated backscatter. Given that the backscatter estimates are uncorrelated from frequency to frequency for both medium locations, the covariance between backscatter estimates for the two locations must be zero unless the frequencies are identical, i.e. if $\hat{BSC}_1(\omega_i)$ and $\hat{BSC}_1(\omega_j)$ are uncorrelated, it follows that $\hat{BSC}_1(\omega_i)$ and $\hat{BSC}_2(\omega_j)$ are also uncorrelated. As a result, Eq. (12) can be simplified to

$$\mathrm{cov}(\hat{a}_1, \hat{a}_2) \approx \sum_{\omega_i} \left( \frac{\partial \hat{a}}{\partial \hat{BSC}(\omega_i)} \right)^2 \langle \hat{BSC}(\omega_i) \rangle^2 \rho_{\mathrm{BSC}}(\omega_i), \tag{13}$$

where the expected value of the backscatter is equivalent to, and has been substituted for, the standard deviation of the backscatter estimator[10] for positions 1 and 2 (legitimate given the earlier assumption that joint-Gaussian statistics apply to the data segment transforms), and the subscripts have been dropped since the quantities involved, other than the backscatter correlation, are independent of spatial position. Finally, using Eq. (10) to calculate the partial derivatives, and dividing the result by the standard deviations of the size estimates, which are also approximated using Eq. (13) where the subscripts are identical, yields (see the Appendix)

$$\rho_a \approx \frac{\Sigma_{\omega_i} (\omega_i^2 - \overline{\omega^2})^2 \rho_{\mathrm{BSC}}(\omega_i)}{\Sigma_{\omega_i} (\omega_i^2 - \overline{\omega^2})^2}, \tag{14}$$

where $\rho_a$ is the correlation between size estimates.

## III. METHOD

### A. Spectral coherence

To test Eq. (9), rf data were simulated for a linear array transducer interrogating a uniform scattering medium.[25] Each of 11 data sets contained 181 rf echo data lines simulated for transducer rotation increments of 0.5 degrees about the transmit focus of the transducer (3 cm) from a minimum angle of 0 degrees to a maximum of 90 degrees. The background medium speed of sound was set to 1540 m/s, and the attenuation to zero for convenience. Scatterers ($4000/\mathrm{cm}^3$) of diameter 50 micrometers were randomly dispersed within the background medium, and their locations reordered for each data set. The transducer aperture was set to 1.5 cm, the center frequency to 5 MHz with 100 percent bandwidth, and neither apodization, dynamic receive focus, nor dynamic aperture were used. However, to simplify the calculation of Eq. (9) while approximating the effects of dynamic receive focus and dynamic aperture, the field amplitude was artificially restricted to be invariant with depth near the transmit focus, i.e., the region from which rf data segments were selected.

For a specified segment length, spectral estimates were produced for each rf line by gating the signal with a rectangular window of that length centered about the rotation center/transmit focus of the transducer, and generating a periodogram with the result. [Although other windows could have been employed, the accuracy of the gating approximation of Eq. (1) may be reduced for some of the more typical types given that it does not take window shape into account.] To estimate spectral coherence as a function of rotation angle and frequency for comparison with Eq. (9), for every spectral frequency point of each data set, covariance was estimated as a function of angle, theta, by pairing the periodogram value for each rf line with the value for the line corresponding to a rotation increment of theta degrees. The covariance estimates were then averaged across data sets to reduce noise, and normalized to produce coherence curves for each frequency point.

Theoretical values were obtained by numerically integrating Eq. (9). Because the simulation incorporated a linear array without apodization, the point-spread function used was sinc $(\sin(\pi x)/(\pi x))$ squared. Since the field amplitude was artificially made invariant in the focal region, only the position and phase of the fields changed over the range of integration. The integration limits were approximated roughly by setting them according to the gate length: $y_{\min} = (-l/2)\cos\varphi$ and $y_{\max} = (l/2)\cos\varphi$.

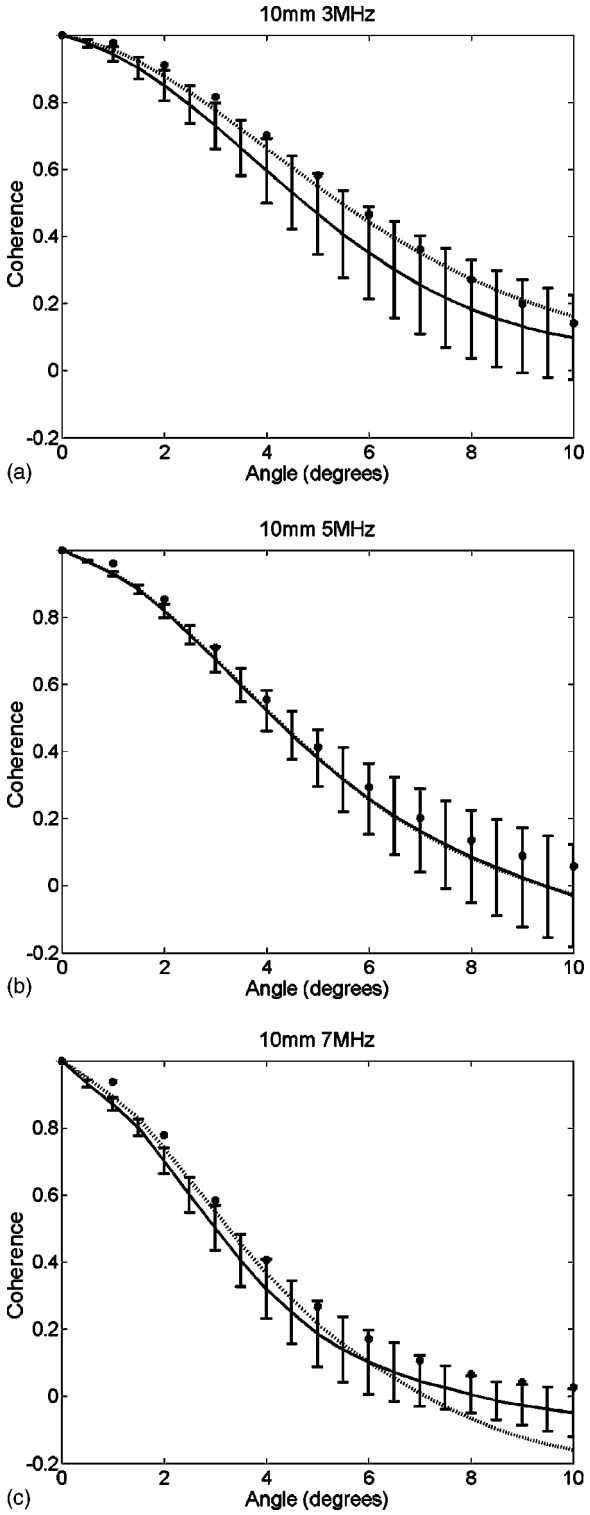


FIG. 2. Spectral coherence versus angle for a gate length of 10 mm and frequencies of (a) 3 MHz, (b) 5 MHz, and (c) 7 MHz. Dots are theoretical values, and solid and dashed lines are the results of simulation experiments.

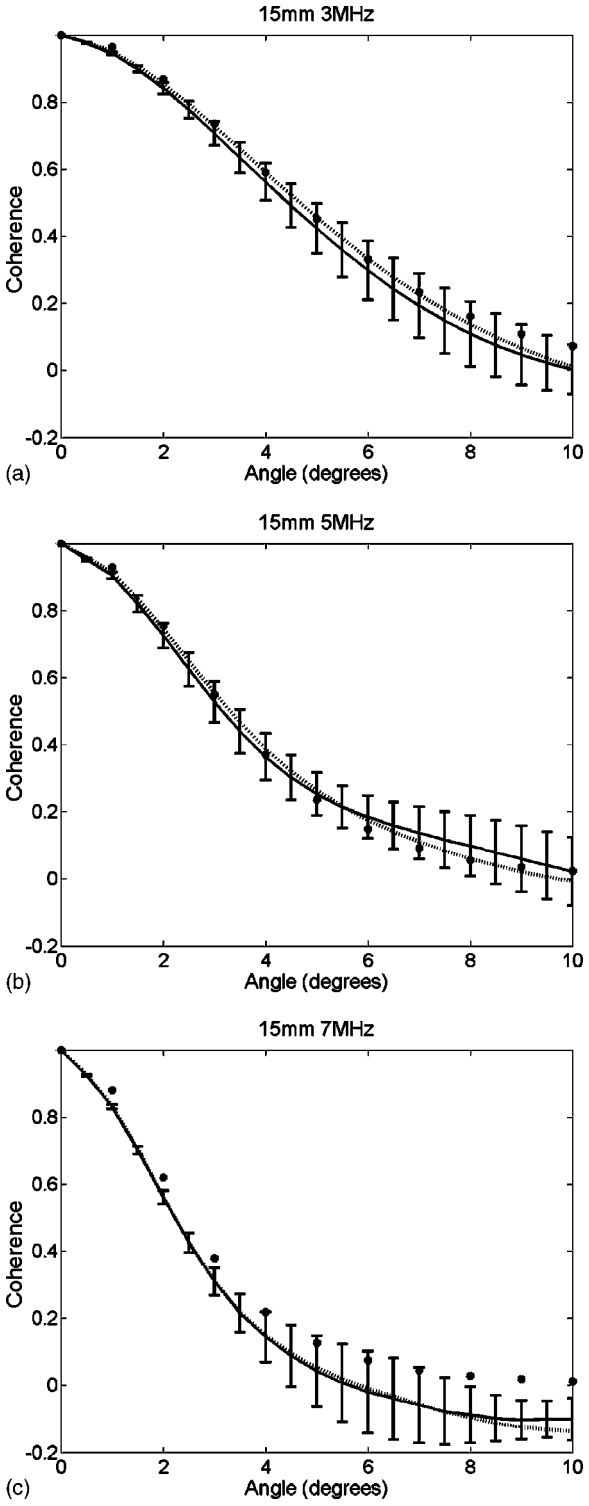


FIG. 3. Spectral coherence versus angle for a gate length of 15 mm and frequencies of (a) 3 MHz, (b) 5 MHz, and (c) 7 MHz. Dots are theoretical values, and solid and dashed lines are the results of simulation experiments.

### B. Size estimate correlation

The accuracy of Eq. (14) was also explored using simulated data. However, rather than use the code of the previous section, for which a backscatter correlation must be calculated, new code was written which would generate pairs of rf Fourier transforms according to a specified function of coherence over frequency. Assuming Rayleigh scattering statistics, this could be done by drawing randomly the real and imaginary parts of the transform for individual frequency points in pairs, corresponding to the two different transducer positions, from a joint-Gaussian distribution with zero mean,[15] $\mathrm{var}=\sqrt{\mathrm{BSC}(\omega)/2}$, and $\rho(\omega)=\sqrt{\rho_{\mathrm{BSC}}(\omega)}$, where, again, $\rho_{\mathrm{BSC}}(\omega)$ was selected. $\mathrm{BSC}(\omega)$ had a functional form

which corresponds to a Gaussian spatial autocorrelation function, where the effective size was also a selected parameter.

Ten data sets of 300 Fourier transform pairs each were generated for several different functions of backscatter correlation. The effective scatterer diameter was set to 75 um, and the bandwidth to 100 percent at a center frequency of 5 MHz. For each backscatter correlation function, a periodogram was produced and the scatterer size estimated for every transform. Scatterer size correlation was then estimated for each data set by pairing the size estimates for each Fourier transform pair. The results were averaged across data sets to reduce estimate noise. Theoretical values, for comparison, were generated numerically according to Eq. (14).

## IV. RESULTS

### A. Spectral coherence

Figures 2 and 3 contain spectral coherence results for two gate lengths and typical frequencies used in size estimation and imaging. For each graph, theoretical and simulation values of coherence are plotted as a function of rotation angle. Dots represent theoretical values, while dashed lines connect simulation results for which averaging, as described in the previous section, was performed across the eleven covariance estimates before normalization. Coherence estimates produced using this method are inherently biased low (i.e., the estimator itself is biased), and become worse as fewer covariance estimates are averaged before normalization. As a result, proper error bars for these values could not be generated by calculating the standard deviation for individual normalized covariance estimates. The results of a separate calculation were therefore included which, although less accurate, allow for error bar generation. Nine of the eleven covariance estimates were divided into three groups of three. Each group of three was averaged and subsequently normalized. Means and standard deviations were then calculated across groups. The results appear as solid lines in the figures. The dashed lines are less biased than the solid lines, but the error bars of the solid lines indicate the general precision of the estimates.

In all cases, the agreement between simulation and theoretical values appears to be good. The coherence estimation bias is believed to be a contributing factor to consistently lower simulation values. However, the disagreement appears to become worse with increasing angle and decreasing frequency for gate lengths shorter than those of Figs. 2 and 3, suggesting that the integration limit approximation described in Sec. III may fail to include significant portions of nonoverlapping acoustic fields in these cases. A more complex treatment of the integration limits and the inclusion of additional, independent data sets may therefore alleviate some of the disagreement.

### B. Size estimate correlation

Figure 4 displays the results for size estimate correlation as a function of the associated coherence between rf Fourier transforms. Two simple cases were explored. The first assumes that backscatter correlation for a given rotation angle is constant with frequency, which is generally expected when the rotated point spread function overlaps significantly with the original over the gated region for all frequencies within the transducer bandwidth (see Sec. V). The second assumes a monotonic decrease of backscatter correlation with frequency, which is commonly expected when the rotated point spread function does not overlap significantly with the original. For the sake of simplicity, a linear decrease in correlation with frequency was assumed for this case. Although some agreement between theory and simulation is evident, the theoretical approximation appears to consistently overestimate the true size estimate correlation. In both cases, the error becomes progressively worse as correlation increases. The source of the error appears to be in the approximation itself [Eq. (14)], and caution is therefore suggested in its use, especially for higher values of correlation.

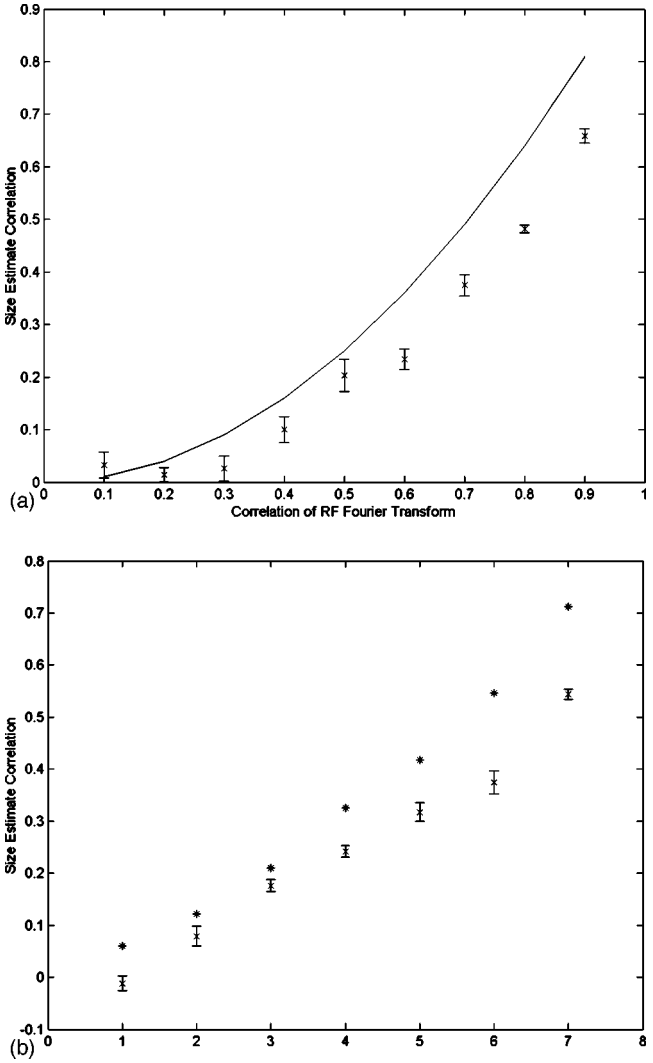


FIG. 4. Size estimate correlation versus rf Fourier transform coherence assuming (a) a constant transform coherence and (b) a linearly decreasing transform coherence with frequency. Minimum and maximum transform coherence values for (b) are as follows: 1: 0.2–0.3, 2: 0.2–0.5, 3: 0.2–0.7, 4: 0.2–0.9, 5: 0.4–0.9, 6: 0.6–0.9, and 7: 0.8–0.9.

## V. DISCUSSION: IMPLICATIONS FOR THE STATISTICAL ANALYSIS AND OPTIMIZATION OF ANGULAR COMPOUNDING

Given sufficient accuracy of the theoretical spectral coherence and size estimate correlation formulas as shown in Figs. 2–4, the statistical analysis and optimization of angular compounding techniques applied to scatterer size estimation and imaging becomes possible. For example, consider the simple case discussed previously, where an aperture is rotated about the location of its transmit focus as in Fig. 1. Assume that rf signals are collected at regular angular intervals, $\Delta\theta$, and that compounding of the data is done after size estimation rather than before, i.e., scatterer size estimates, as opposed to spectral or backscatter estimates, are averaged. Using Eq. (9) in conjunction with Eq. (14), an expression for the correlation between size estimates as a function of angular separation, $\rho_{\hat{a}}(n\,\Delta\theta)$, for a specific set of ultrasonic system parameters, can be derived. Assuming that a total of $N$ signals are recorded, corresponding to a maximum compounding angle of $N\,\Delta\theta$, the theoretical improvement in the size estimate SNR after compounding is given by[16]

$$\frac{\mathrm{SNR}_{\mathrm{comp}}}{\mathrm{SNR}}=\left[\sqrt{\frac{1}{N}+2\sum_{n=1}^{N}\frac{(N-n)}{N^2}\rho_{\hat{a}}(n\,\Delta\theta)}\right]^{-1}. \quad (15)$$

By analyzing this value as a function of system parameters and angular increment, it becomes possible not only to design compounding experiments with the desired level of effectiveness (as quantified by the SNR) without correlation measurements, but also to optimize these parameters in order to maximize performance.

Although statistical analysis and optimization can always be done numerically, it is difficult in general to determine, analytically, the dependencies of spectral coherence, size estimate correlation, and size estimate SNR upon system parameters. However, for the simple case described above, a few assumptions and simplifications can be introduced that make analytical progress possible. This, in turn, allows for some general conclusions regarding the use and optimization of angular compounding to be made, connects this work with that done for speckle, and provides insight into the physical mechanisms responsible for size estimate decorrelation. Minimizing size estimate correlation as a function of angular separation is generally necessary for optimizing compounded size estimate/image SNR, and is the case for the simple set-up under consideration here based upon the form of Eq. (15). The following analysis will therefore focus both upon the first steps toward obtaining an analytical solution for size estimate correlation as a function of angle and the adjustment of experimental parameters for its minimization.

Assume, for the sake of simplicity, that the point-spread function for the system is adequately represented by a sinc squared function, and that the amplitude of the field, as earlier, does not vary significantly in the axial direction near the transmit focus.

Approximating the distance in the phase of Eq. (9) as $-bx/z_0$ yields[18]

$$\rho_{1,2}(\omega)\approx\frac{\int_{\Omega_{1,2}}dx\,dy\,\mathrm{sinc}^2\left[\frac{D}{z_0\lambda}(x\cos\varphi-y\sin\varphi)\right]\mathrm{sinc}^2\left[\frac{D}{z_0\lambda}(x\cos\varphi+y\sin\varphi)\right]e^{-2ki(bx/z_0)}}{\int_{\Omega_{1,2}}dx\,dy\,\mathrm{sinc}^4\left(\frac{Dx}{z_0\lambda}\right)}, \quad (16)$$

for the coherence between Fourier transformed segments, where $D$ is the transducer aperture width, $\lambda$ is the wavelength which corresponds to wavenumber $k$, $z_0$ is the distance from the transducer to the transmit focus, and $b$ is again the distance from position 1 to position 2 (see Fig. 1). From here, two simplifying assumptions can be made which will be considered separately. First, the dependence of the point-spread function position upon rotation angle will be neglected by using the approximation $\varphi\approx 0$. Assuming that the integration limits can be adequately handled by limiting integration in the $y$-direction from $-l/2$ to $l/2$ gives

$$\rho_{1,2}(\omega)\approx\frac{\int dx\,\mathrm{sinc}^4\left(\frac{Dx}{z_0\lambda}\right)e^{-2ki(bx/z_0)}}{\int dx\,\mathrm{sinc}^4\left(\frac{Dx}{z_0\lambda}\right)}. \quad (17)$$

This is simply a normalized, one-dimensional Fourier transform, and is equivalent to the result, studied in detail by both Wagner and O'Donnell,[16,18] obtained for speckle correlation. To distinguish this result from the next, hereafter it will be referred to as phase decoherence (i.e., loss of coherence with angle), since any deviation from complete coherence is the result of a nonzero rotation angle contained in the phase term. The physical mechanism responsible for this type of decoherence is the change in position, relative to the transducer aperture, of scatterers contained within the gated, insonifying beam as the aperture rotates. The phase decoherence mechanism tends to be the dominant source of decoherence when the beam overlaps its original location significantly with rotation.

Without going into the details of the solution to Eq. (17), the result, like most correlation curves, starts at one for a zero rotation angle, and falls to zero as the angle increases. As both Wagner and O'Donnell indicate, it is a function of

$$\frac{b}{D}\approx\frac{\theta}{D/z_0}. \quad (18)$$

The characteristic length of the phase decoherence curve is,

therefore, completely independent of frequency and gate length, but proportional to the aperture size and inversely proportional to the depth of the transmit focus. In essence, this result indicates that wider fields lead to quicker decoherence, and thus a more rapid decorrelation of size estimates with angle, when the phase term is the source of that decoherence. With wider fields, more scatterers away from the rotation center, where the relative change in position with aperture rotation is greater, contribute to the rf signal. However, the invariance of Eq. (17) with frequency indicates that changes in field width due to frequency shifts are negated by offsetting changes to the frequency dependent phase term.

The second case neglects decoherence due to phase changes completely and considers decoherence due to beam movement [i.e., the change in position of the field amplitude term of Eq. (16) with rotation] only by utilizing the approximation $b \approx 0$, $\cos\varphi \approx 1$:

$$\rho_{1,2}(\omega) \approx \frac{\int_{\Omega_{1,2}} dx\, dy\, \mathrm{sinc}^2\left[\frac{D}{z_0\lambda}(x - y\sin\varphi)\right]\mathrm{sinc}^2\left[\frac{D}{z_0\lambda}(x + y\sin\varphi)\right]}{\int_{\Omega_{1,2}} dx\, dy\, \mathrm{sinc}^4\left(\frac{Dx}{z_0\lambda}\right)}, \tag{19}$$

where the integration limits will be handled as before. The numerator is simply a convolution of the sinc squared function in the $x$-direction, and an integration of the result in the $y$-direction. The decoherence associated with this approximation, hereafter, will be referred to as field amplitude decoherence. The primary physical mechanism responsible for this type of decoherence is the incorporation of new scatterers within, and exclusion of old scatterers from, the beam as it rotates about the center of the gated region. This mechanism tends to be the dominant source of decoherence when the field amplitude rotates off its original position quickly.

Without generating an analytical solution, it can be demonstrated that Eq. (19) is a function of

$$\frac{lD2\sin\varphi}{z_0\lambda} \approx \frac{lD\theta}{z_0\lambda}. \tag{20}$$

Making the change of variable $x = (\lambda z_0/D)x' - y\sin\varphi$, the numerator of Eq. (19) becomes

$$\int_{-l/2}^{l/2}\int_{-\infty}^{\infty}\frac{\lambda z_0}{D}\mathrm{sinc}^2\left(\frac{2D}{\lambda z_0}y\sin\varphi - x'\right)\mathrm{sinc}^2(x')\,dx'\,dy. \tag{21}$$

Integrating yields

$$\int_{-l/2}^{l/2}\frac{\lambda z_0}{D}f\left(\frac{2D}{\lambda z_0}y\sin\varphi\right)dy, \tag{22}$$

where $f$ is the convolution of $\mathrm{sinc}^2$. Integrating again produces

$$\frac{\lambda z_0 l}{DC}[F(C/2) - F(-C/2)], \tag{23}$$

where $C$ is the quantity of Eq. (20) and $F$ is the integral of $f$. Upon normalization, Eq. (23) becomes a function of $C$ alone.

In contrast to the previous results for phase decoherence, Eq. (20) indicates that narrower fields yield faster field amplitude decoherence. Essentially, narrower fields tend to separate from their original positions to incorporate new scatterers and exclude old ones much more quickly with rotation than broader fields. The characteristic length of the field amplitude decoherence is also inversely proportional to gate length. The larger the gate, the more nonoverlapping field is generally included in the numerator integral of Eq. (19).

The results for field amplitude and phase decoherence suggest some general principles for the minimization of size estimate correlation as a function of angle. Practically, external constraints on experimental parameters, due to resolution requirements for example, restrict any given system to operation in a specific region of parameter space. If the mechanism responsible for phase decoherence is negligible within that region, then the minimization conditions discussed for field amplitude decoherence (i.e., maximally narrow beams and long gates) minimize both the total decoherence of Eq. (16) and, with adjustments to account for the frequency dependent weighting of Eq. (14), size estimate correlation. Conversely, if the mechanism responsible for field amplitude decoherence is negligible, then the phase decoherence minimization conditions apply for minimizing the total decoherence and size estimate correlation [the weighting of Eq. (14) is irrelevant in this case since phase decoherence is frequency independent].

In reality, however, both mechanisms will generally contribute to the total decoherence with aperture rotation. If this is indeed the case, then minimizing conditions may be more complex. One physical mechanism will often dominate changes to the total decoherence as parameters are adjusted within a particular parameter space, in which case the minimizing conditions of that mechanism will apply. However, a local maximum or minimum in total decoherence may exist within the open parameter space where, regardless of parameter changes, total decoherence either exclusively increases or decreases. In such cases, as with any similar optimization problem, either the location of the local minimum or the boundaries of the open parameter space will determine the total decoherence minimization conditions.

It should be noted that if the field amplitude decoherence mechanism is a source of decoherence for a given set of parameters, an inherent loss of resolution accompanies the

implementation of angular compounding. This is due to the fact that, upon rotation, new scatterers located within neighboring resolution cells contribute significantly to the echo signal. Different spatial compounding techniques (e.g., compounding estimates from parallel beams), which degrade resolution to a corresponding degree, may therefore be just as effective as, and perhaps easier to implement than, angular compounding in instances where the phase decoherence mechanism contributes little to the total decoherence. In contrast, little to no resolution is lost when phase decoherence is predominant. Regardless of the rotation angle, here it is the same scatterers, located within a single resolution cell, which produce the echo signal. As a result, if angular compounding is being considered for a system and set of parameters for which the field amplitude decoherence mechanism is significant yet losses in resolution are unacceptable, then angular compounding should not be implemented. However, if the phase decoherence mechanism is the sole source of decoherence, then angular compounding will only be beneficial.

## VI. CONCLUSION

General expressions for the correlation between backscatter coefficient and scatterer size estimates, generated for the same tissue location but from different angles of incidence, were derived and compared against simulation results. These formulas can be used to determine the relationships between experimental system parameters and measures of performance such as SNR, making technique optimization possible at the theoretical level.

In general, two different mechanisms appear to be the sources of rotation decoherence between spectral estimates. The first is the change of relative scatterer position with aperture rotation, which is responsible for changes in the phase term of Eq. (16). The second is the change in position of the acoustic field itself, such that successive rotated fields separate from prior ones. These two mechanisms generally affect the total decoherence in an opposing manner with changing experimental parameters, making optimization conditions dependent upon the dominant source of the change in combined decoherence. Although both phase and field amplitude spectral decoherence ultimately result in improved SNR for compounded size estimates, it should be noted that there is an inherent loss of resolution associated with field amplitude decoherence. As a result, angular compounding may not significantly outperform other spatial compounding techniques that trade image resolution for SNR in cases where phase decoherence is insignificant.


## ACKNOWLEDGMENTS

This work was supported in part by NIH Grants No. R21EB002722 and No. T32CA09206.


## APPENDIX: FIELD INTEGRALS AND DERIVATION OF EQ. (14)

### 1.

The field integrals, which first appear in Eq. (1), have the form

$$A_t(\mathbf{r},\omega)=\int_S d\mathbf{r}'\, K_t(\mathbf{r}')\,\frac{e^{ik|\mathbf{r}-\mathbf{r}'|}}{|\mathbf{r}-\mathbf{r}'|}\,e^{-\alpha(\omega)|\mathbf{r}-\mathbf{r}'|},$$

$$A_r(\mathbf{r},\omega)=\int_S d\mathbf{r}'\, K_r(\mathbf{r}',|\mathbf{r}-\mathbf{r}'|)\,\frac{e^{ik|\mathbf{r}-\mathbf{r}'|}}{|\mathbf{r}-\mathbf{r}'|}\,e^{-\alpha(\omega)|\mathbf{r}-\mathbf{r}'|},$$

where the integration is over the face of the transducer ($S$), $K_t$ contains transmit phase and amplitude modifying terms, such as those for apodization and transmit focusing, and $K_r$ contains analogous receive terms, including those for dynamic receive focusing, dynamic aperture, and apodization. $\alpha(\omega)$ is the medium attenuation, and $k$ is the wavenumber corresponding to $\omega$.

### 2.

Using Eq. (10) to calculate the partial derivative for Eq. (13) yields

$$\frac{\partial\hat{a}}{\partial\hat{\mathrm{BSC}}(\omega_i)}=\frac{-d_1^2c^2}{80}\,\frac{(\omega_i^2-\overline{\omega^2})}{\sum_{\omega_{\min}}^{\omega_{\max}}(\omega^2-\overline{\omega^2})^2}\,\frac{10}{\langle\hat{\mathrm{BSC}}(\omega_i)\rangle}\,\frac{1}{2\hat{a}},$$

where, as described in the text, the derivative has been evaluated at the expected value of the backscatter estimator. Inserting this expression into Eq. (13) gives

$$\mathrm{cov}(\hat{a}_1,\hat{a}_2)\approx\left(\frac{-d_1^2c^2}{80}\right)^2\left(\frac{10}{2\hat{a}}\right)^2\frac{\sum_{\omega_i}(\omega_i^2-\overline{\omega^2})^2\rho_{\mathrm{BSC}}(\omega_i)}{[\sum_{\omega_{\min}}^{\omega_{\max}}(\omega^2-\overline{\omega^2})^2]^2}.$$

Thus,

$$\mathrm{var}(\hat{a})\approx\left(\frac{-d_1^2c^2}{80}\right)^2\left(\frac{10}{2\hat{a}}\right)^2\frac{1}{[\sum_{\omega_{\min}}^{\omega_{\max}}(\omega^2-\overline{\omega^2})^2]}$$

and dividing the covariance by the variance yields the correlation of Eq. (14).


[1] T. Hall, M. Insana, L. Harrison, and G. Cox, "Ultrasonic measurement of glomerular diameters in normal adult humans," Ultrasound Med. Biol. **22**, 987–997 (1996).

[2] M. Insana, "Modeling acoustic backscatter from kidney microstructure using an anisotropic correlation function," J. Acoust. Soc. Am. **97**, 649–655 (1995).

[3] M. Insana, "Ultrasonic imaging of microscopic structures in living organs," Int. Rev. Exp. Pathol. **36**, 73–92 (1996).

[4] M. Insana, R. Wagner, D. Brown, and T. Hall, "Describing small-scale structure in random media using pulse-echo ultrasound," J. Acoust. Soc. Am. **87**, 179–192 (1990).

[5] M. Insana, T. Hall, J. Wood, and Z.-Y. Yan, "Renal ultrasound using parametric imaging techniques to detect changes in microstructure and function," Invest. Radiol. **28**, 720–725 (1993).

[6] M. F. Insana, T. J. Hall, and J. L. Fishback, "Identifying acoustic scattering sources in normal renal parenchyma from the anisotropy in acoustic properties," Ultrasound Med. Biol. **17**, 613–626 (1991).

[7] M. F. Insana, J. G. Wood, and T. J. Hall, "Identifying acoustic scattering sources in normal renal parenchyma in vivo by varying arterial and ureteral pressures," Ultrasound Med. Biol. **18**, 587–599 (1992).

[8] M. L. Oelze, J. F. Zachary, and J. William D. O'Brien, "Parametric imaging of rat mammary tumors *in vivo* for the purposes of tissue characterization," J. Ultrasound Med. **21**, 1201–1210 (2002).

[9] R. L. Romijn, J. M. Thijssen, and G. W. J. V. Beuningen, "Estimation of scatterer size from backscattered ultrasound: A simulation study," IEEE Trans. Ultrason. Ferroelectr. Freq. Control **36**, 593–606 (1989).

[10] P. Chaturvedi and M. Insana, "Error bounds on ultrasonic scatterer size estimates," J. Acoust. Soc. Am. **100**, 392–399 (1996).

[11] A. Gerig, J. Zagzebski, and T. Varghese, ''Statistics of ultrasonic scatterer size estimation with a reference phantom,'' J. Acoust. Soc. Am. **113**, 3430–3437 (2003).
[12] M. L. Oelze, J. F. Zachary, and W. D. O'Brien, ''Characterization of tissue microstructure using ultrasonic backscatter: Theory and technique for optimization using a Gaussian form factor,'' J. Acoust. Soc. Am. **112**, 1202–1211 (2002).
[13] F. Lizzi, E. Feleppa, M. Astor, and A. Kalisz, ''Statistics of ultrasonic spectral parameters for prostate and liver examinations,'' IEEE Trans. Ultrason. Ferroelectr. Freq. Control **44**, 935–942 (1997).
[14] F. L. Lizzi, M. Astor, E. J. Feleppa, M. Shao, and A. Kalisz, ''Statistical framework for ultrasonic spectral parameter imaging,'' Ultrasound Med. Biol. **23**, 1371–1382 (1997).
[15] R. F. Wagner, S. W. Smith, J. M. Sandrik, and H. Lopez, ''Statistics of speckle in ultrasound B-scans,'' IEEE Trans. Sonics Ultrason. **30**, 156–163 (1983).
[16] M. O'Donnell and S. D. Silverstein, ''Optimum displacement for compound image generation in medical ultrasound,'' IEEE Trans. Ultrason. Ferroelectr. Freq. Control **35**, 470–476 (1988).
[17] G. E. Trahey, S. W. Smith, and O. T. V. Ramm, ''Speckle pattern correlation with lateral aperture translation: Experimental results and implications for spatial compounding,'' IEEE Trans. Ultrason. Ferroelectr. Freq. Control **33**, 257–264 (1986).
[18] R. Wagner, M. Insana, and S. Smith, ''Fundamental correlation lengths of coherent speckle in medical ultrasonic images,'' IEEE Trans. Ultrason. Ferroelectr. Freq. Control **35**, 34–44 (1988).
[19] R. R. Entrekin, B. A. Porter, H. H. Sillesen, A. D. Wong, P. L. Cooperberg, and C. H. Fix, ''Real-time spatial compound imaging: Application to breast, vascular, and musculoskeletal ultrasound,'' Semin Ultrasound CT MR **22**, 50–64 (2001).
[20] A. L. Gerig, T. Varghese, and J. A. Zagzebski, ''Improved parametric imaging of scatterer size estimates using angular compounding,'' IEEE Trans. Ultrason. Ferroelectr. Freq. Control **51**, 708–715 (2004).
[21] J.-F. Chen, J. Zagzebski, F. Dong, and E. Madsen, ''Estimating the spatial autocorrelation function for ultrasound scatterers in isotropic media,'' Med. Phys. **25**, 648–655 (1998).
[22] M. Insana and D. Brown, ''Acoustic scattering theory applied to soft biological tissues,'' in *Ultrasonic Scattering in Biological Tissues*, edited by K. Shung (CRC Press, Boca Raton, 1993), pp. 75–124.
[23] A. Macovski, *Medical Imaging Systems* (Prentice–Hall, Upper Saddle River, NJ, 1983).
[24] P. Bevington and K. Robinson, *Data Reduction and Error Analysis for the Physical Sciences*, 2nd ed. (McGraw-Hill, New York, 1992).
[25] Y. Li and J. A. Zagzebski, ''A frequency domain model for generating B-mode images with array transducers,'' IEEE Trans. Ultrason. Ferroelectr. Freq. Control **46**, 690–699 (1999).